Accepted Manuscript

Title: Pd-γAl$_2$O$_3$ Applied to Tryglicerides Hydrogenation with Supercritical Propane. Experimental and Theoretical Catalysts Characterization

Authors: C.M. Piqueras, I.O. Costilla, P.G. Belelli, N.J. Castellani, D.E. Damiani

Please cite this article as: C.M. Piqueras, I.O. Costilla, P.G. Belelli, N.J. Castellani, D.E. Damiani, Pd-γAl$_2$O$_3$ Applied to Tryglicerides Hydrogenation with Supercritical Propane. Experimental and Theoretical Catalysts Characterization, *Applied Catalysis A, General* (2007), doi:10.1016/j.apcata.2008.05.029

This is a PDF file of an unedited manuscript that has been accepted for publication. As a service to our customers we are providing this early version of the manuscript. The manuscript will undergo copyediting, typesetting, and review of the resulting proof before it is published in its final form. Please note that during the production process errors may be discovered which could affect the content, and all legal disclaimers that apply to the journal pertain.

Pd-γAl$_2$O$_3$ Applied to Tryglicerides Hydrogenation with Supercritical Propane. Experimental and Theoretical Catalysts Characterization
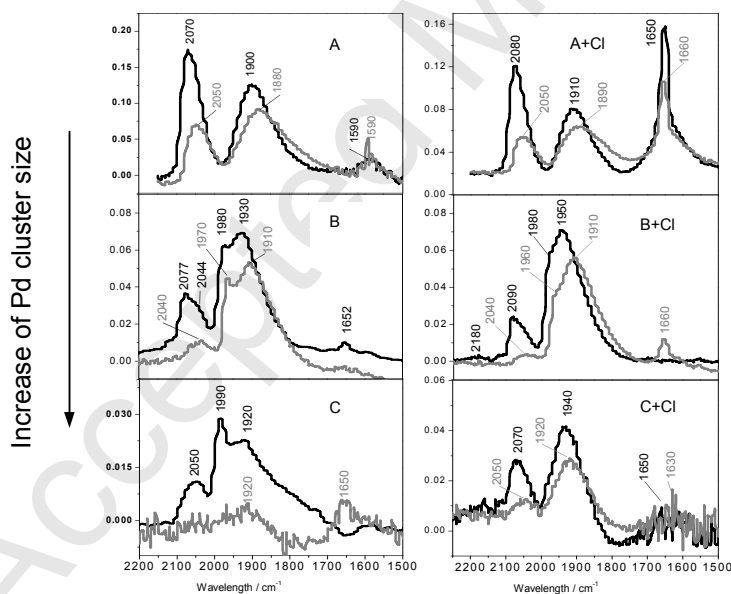
C. M. Piqueras[1]*, I. O. Costilla[1], P. G. Belelli [2], N. J. Castellani [2], D. E. Damiani[1]

[1] PLAPIQUI (UNS-CONICET), Camino La Carrindanga km 7, CC 717, 8000, Bahía

Blanca, Argentina, Tel. 54-291-4861700,

[2] Departamento de Física – Universidad Nacional del Sur (UNS) Av. Alem 1253, 8000

Bahía Blanca, Argentina. *email: cpiqueras@plapiqui.edu.ar

FTIR spectra of CO adsorption on Pd-Al$_2$O$_3$ catalysts

Pd-γAl$_2$O$_3$ catalysts with different metallic particle size and modified with Cl were used in the trygliceride hydrogenation. The experiences were carried out in homogeneous-phase conditions using supercritical propane. FTIR spectra's and DFT calculations evidenced the enhancement of the CO adsorption energy due to the presence of electro deficient ensembles. These lasts could promote the modification of the reaction selectivity and (TOF) values.

Pd-γAl₂O₃ Applied to the Hydrogenation of Triglycerides with Supercritical Propane. Experimental and Theoretical Characterization of Catalysts

C. M. Piqueras[1]*, I. O. Costilla[1], P. G. Belelli [2], N. J. Castellani [2], D. E. Damiani[1]

[1] PLAPIQUI (UNS-CONICET), Camino La Carrindanga km 7, CC 717, 8000, Bahía Blanca, Argentina, Tel. 54-291-4861700,

[2] Departamento de Física – Universidad Nacional del Sur (UNS) Av. Alem 1253, 8000 Bahía Blanca, Argentina. *email: cpiqueras@plapiqui.edu.ar

Abstract

A set of Pd-γAl₂O₃ catalysts of different metallic particle sizes and modified with 2-chloro-butane was used for triglyceride hydrogenation. The experiments were carried out in single-phase conditions using propane as a supercritical solvent. A generalized criterion was used to determine the absence of mass-transfer limitations for both reactants inside the pore structure of the catalyst.

FTIR spectra of CO on diverse catalysts showed different absorption bands and significant shifts to higher wavelengths of the CO species corresponding to on-top and bridge configurations. In order to test these results, theoretical studies using the density functional theory (DFT) were carried out for the FTIR of CO

adsorption on two Pd ensembles, with or without charge deficiency and with Cl adsorbed on them. The results showed similar displacements of the band frequencies to those obtained experimentally, and demonstrate an enhancement of the CO adsorption energy of the on-top, isolated bridge and three-fold bridge CO species on electron deficient ensembles. Enhancement of the adsorption bond strength could promote the direct hydrogenation of the diunsaturated compound to complete saturated fatty acid chains. The decrease of the specific reaction rate (TOF) and the increase of the saturated fatty acids production, as well as a decrease of the monounsaturated and isomers content observed is in line with a possible modification of the electronic properties of the Pd particles. The influence of some planes of Pd clusters intervening on the direct hydrogenation is discussed.

1. Introduction

The hydrogenation of high molecular weight substrates, as triglycerides, is carried out in a three phase process (gas–liquid–solid). It is controlled by the availability of hydrogen at the catalyst surface, which in turns is limited by both the low solubility of hydrogen and the high mass transfer resistance of the liquid phase [1]. In this way, the efficiency of the catalyst is lowered and the reaction is not sensitive to the metallic surface disposition on the catalyst (a "facile" reaction)[2,3]. Furthermore the hydrogen scarcity favours side reactions, such as double bond transposition and *cis-trans* isomerization in the triglyceride partial hydrogenation [4]. On this specific subject, there is an increasing concern due to the fact that *trans* fatty acids are harmful to human health [5]. Therefore the development of new technologies to minimize the production of *trans* isomerization during hydrogenation is of current interest [6].

The application of supercritical fluids to these reactions reduces the mass-controlling step by eliminating the gas–liquid interface and by increasing the diffusivity of reactants and products [7]. Therefore, the reaction could be carried out in kinetic reaction regime with two main advantages: the rate and the selectivity could be affected by the shape of the metal catalyst and they might be improved by manipulating the process variables (temperature, H_2 concentration, and so on). For instance, while gas–liquid hydrogenation reactions seem to be insensitive to the catalyst surface shape and require high temperatures to increase hydrogen solubility; the temperature of the supercritical process can be modified with no effects in the reactants compositions [8].

Some examples of the application of supercritical fluids to several processes were reported, including cases where isomerization reactions, favoured by the lack of hydrogen at the catalyst surface, were partially avoided [9]. Other authors showed that the enhancement of conversion and selectivity for the hydrogenation of ortho- and meta-cresol,

3

was attained by varying system variables [10]. The application of supercritical fluids helps in solving selectivity problems in enantioselective hydrogenations demonstrated in the literature, raising the isomeric resolution [11,12]. Other authors carried out hydrogenation of unsaturated aldehydes in supercritical CO_2, obtaining very high selectivities with a simple monometallic catalyst like Pt supported on alumina [13]. Finally the hydrogenation of vegetable oils and fatty acid esters, under supercritical conditions were studied [9,14]. These authors reported a statistical experimental research varying several key variables, observing a number of orders of magnitude increase in the reaction rate and an improvement of the selectivity, compared to conventional hydrogenation results.

To our knowledge, there is no information about using supercritical fluid technology on the catalyst design to improve the reaction selectivity. Some of us [15], reported the influence of the metallic particle size on the selectivity and specific activity of the triglyceride hydrogenation, and also demonstrated that the use of supercritical propane could bring the global rate to the reaction kinetic regime. In that case, the surface reaction exhibited a tendency to depend on the metallic particle size, where *trans* isomers content as well as specific activity were directly linked to the cluster diameter. In the present work more evidence and a deeper discussion about the reaction pathway is proposed with the help of DFT calculations and FTIR measurements. Additional data to the proposed hypothesis is collected when the catalysts are modified with 2-chloro-butane.

2. Experimental

2.1 Materials

Propane (99.01% molar) provided by TGS, Bahía Blanca, Argentina, was used as the reaction solvent. Chromatographic-grade (99.999 % molar) hydrogen, chromatographic-grade (99.999 % molar) nitrogen, analytical-grade (99.99% molar) air,

argon, and helium (5.0 ultra-pure grade), were provided by AGA, Argentina. The triglycerides mixture was a refined, bleached, and deodorized commercial sunflower oil, with initial fatty acids composition 7.94% C16.0 (palmitic), 4.22% C18.0 (stearic), 23.06% C18.1 (oleic), 64.44% C18.2 (linoleic), 0.17% C18.3 (linolenic), 0.54% C20.0 (eicosanoic), 0.64% C22.0 (docosanoic), maintained in an nitrogen atmosphere and used without previous treatment. The support was γ-Al$_2$O$_3$ (Condea Puralox, 148 m^2 g^{-1}, 74 μm particle diameter, average pore size 9 nm and pore volume 0.005 cm^{3}g^{-1}). The metal precursors were palladium acetylacetonate Pd(C$_5$H$_7$O$_2$)$_2$, provided by Alpha, and palladium nitrate Pd(NO$_3$)$_2$, which was supplied by Sigma.

2.2 Catalyst Preparation and Characterization

A and B catalysts were prepared by impregnation of the γ-Al$_2$O$_3$ support with a solution of (Pd(C$_5$H$_7$O$_2$)$_2$) in toluene, using 5 times the total pore volume as impregnation volume. The solution had a Pd concentration equal to 1.1 times the Pd concentration required to leave a nominal 0.5% and 1% wt/wt Pd loading on the support respectively. After impregnation, the catalyst was dried at room temperature for 72 h, then in an Ar atmosphere at 423 K for 2 h and finally calcined in a flow (100 cm^3 min^{-1}) of chromatographic air at 673 K during 2 h. The C catalyst was prepared by the incipient wetness method, using (Pd(NO$_3$)$_2$) solution as a metal precursor. The support was slowly contacted with the impregnating solution. The Pd concentration was adjusted in order to give a metal loading of 1% wt/wt on the support. The catalyst was dried for 24 hours at room temperature; and afterwards it was calcined for 2 hours at 773 K in chromatographic air. The D catalyst was prepared by reducing catalyst C in H$_2$, heating the sample at a 5 K min^{-1} rate from 298 K to 573 K and allowing the sample to remain at this final temperature during 1 hour. This treatment produces a sintering of the Pd clusters [16].

In order to modify the metal behavior and following the idea of Botiaux et al. [17,18] 2-chloro-butane was added to this set of catalysts by wet impregnation in a 5:1 Cl:Pd molar ratio. The resulting samples were named as A+Cl, B+Cl and C+Cl. Afterwards the catalysts were calcined at 723 K for 2.5 h. All of them were reduced in H_2 flux at 373 K during 1 h previous to the reaction, and protected with a cover of 100 mg of hard-hydrogenated triglyceride (IV=45, Iodine Value defined as grams of I_2 consumed per 100 g of oil).

The metal content was determined by atomic absorption spectrometry (Instrumentation Laboratory 551). Specific surface areas were evaluated by the BET method on a volumetric system Nova 1200e Quantachrome Instruments, with nitrogen as adsorbing gas at 77 K. The H_2 chemisorption uptakes were measured in a conventional glass apparatus [19]. Before reduction, the catalysts were oxidized in air at 773 K during 1 hour. Then, the samples were purged in He and reduced at 523 K in flowing H_2 for 1 hour. Following the reduction, the samples were evacuated for 2 hours at reduction temperature and cooled to adsorption temperature (298 K) under vacuum. Irreversible hydrogen uptakes were determined from dual isotherms measured for hydrogen using Benson et al.´s double-isotherm method [20]. The fraction of exposed palladium was calculated assuming a 1:1 hydrogen atom adsorbed per surface palladium atom stoichiometry.

FTIR studies of adsorbed CO were carried out at 313 K using a Nicolet 20DXB spectrometer with a resolution of 4 cm^{-1}. Wafers of 1.2 cm diameter were prepared under a pressure of 4.2 Ton cm^{-2}. The average weight of the wafers was 22 mg cm^{-2}. The pellets were placed in a stainless steel IR cell equipped with CaF_2 windows. The cell allows in situ oxidation with chromatographic air at 573 K for 2 h and reduction under 700 Torr of H_2 at 393 K during 1 h. After that the samples were evacuated at the calcination temperature. Once the IR spectrum of the clean surface sample was obtained, the catalyst was

equilibrated with 5 Torr of CO at 313 K and the spectrum was recorded after 20 min of catalyst exposition, adding 150 scans. Finally the samples were evacuated (10^{-4} Torr) during 30 min and IR spectra were recorded again in order to compare the amount of CO remaining adsorbed at the surface, as an indicator of the Pd-C bond strength.

2.3. Catalytic measurements

All the experiments were carried out in a variable volume cell previously reported [21], operated at 373 K and 165 bar. Under these conditions, propane is in supercritical state and the ternary mixture in a single homogeneous phase. The description of the phase equilibria of this ternary mixture as well as the theoretical tools for the calculation of critical lines, have been reported in the literature [22-24],. With these tools the single-phase condition could be verified for each sample during the entire reaction [15]. In all these cases the initial reactant mixture has a molar composition of $7.5\%H_2$/ $90\%C_3H_8$ /2.5% TG, with an initial volume of 19.8 cm^3 approximately. Seven samples were withdrawn during the reaction for verifying the reaction advance. Conversion was calculated from the quantitative analysis of the triglycerides carried out by gas liquid capillary chromatography following the procedure established by the standard method AOCS Ce 1c-89. The iodine value (IV) was calculated from the fatty acids composition according to the norm AOCS Cd 1c-85. In the experiments, 6 to 22 mg of catalyst were used depending on the metal dispersion.

3. Theoretical Calculation of CO adsorption

The Pd particles sizes experimentally found can be classified mainly in two groups: large particles (Dp>4nm) and small particles (Dp<2 nm). The former are characterized by a small number of low coordination sites per unit surface area, while the latter present a

relatively large quantity of them. In order to study the influence on the Pd adsorptive properties of such a geometric factor, two models were considered. The first one, a cluster constructed with 19 Pd atoms, was used to simulate the interaction between the CO molecule and a compact (111) exposed plane belonging to a large Pd particle. The atoms were distributed in two layers, following the C_{3V} symmetry (Figure 1a), and were placed at the bulk positions with a lattice constant of 3.89Å [25]. The adsorption of CO on Pd was analyzed modelling the metallic surface with the cluster method. Particularly, the vibrational frequencies calculated for the CO molecule adsorbed on monometallic Pt [26], CO and NO molecules on Pd and on bimetallic PdCu clusters [27], or bigger adsorbates as the ethylene molecule adsorbed on Pd(111) [28] are in good agreement with the experimental data. The second model, an icosahedral cluster made-up by 13 Pd atoms, was used to simulate the interaction between CO and a highly faceted Pd particle. This cluster was designed comprising a central atom and a first shell of 12 atoms (Figure 1b).

On these models of particle, CO was adsorbed on one-fold and two-fold sites, this molecule having an end-on orientation with the C atom pointing to the cluster. The following adsorptive properties were calculated: geometrical parameters, adsorption energies and vibrational frequencies. The C-O vibrational frequency is one of the most interesting features of our theoretical approach because it can be compared with experimental values measured by IR spectroscopy. Before CO adsorption, the three central Pd atoms of the first layer in the Pd_{19} cluster were relaxed; on the other hand, a full geometry optimization was performed for the Pd_{13} cluster. During the adsorption, the metal atoms were kept at the optimized positions for bare clusters. The CO geometry was fully relaxed. Negligible modifications of the adsorptive parameters were obtained when the surface relaxation was performed together with that of CO geometry.

From the electrostatic point of view, three different situations were considered for the Pd clusters: neutral Pd clusters, positively charged Pd clusters and chemically modified Pd clusters. In the second case, the positively charged Pd clusters imitate the electron-attracting effect of the support. In the third case, the Cl atom is coadsorbed with CO in order to simulate the behaviour of Pd catalysts modified with Cl. Due to fact that the C-O vibrational frequency is highly sensitive to the oxidation state of the metal, the frequency displacement is an interesting tool to analyse the change in the oxidation state undergone by metal atoms.

The molecular orbital calculations have been performed within the density functional theory (DFT) using the hybrid B3LYP exchange-correlation functional [29] as implemented in the Gaussian03 software package [30]. This method has been widely used to study adsorption processes, yielding reliable results on semiconductor [31], oxide [32] as well as metal clusters [33,34]. For example, recently the associative desorption of hydrogen or deuterium molecules from the Ru(001) and the chemisorption of the methoxy radical on the same surface were considered. In the last case, the species was preferentially chemisorbed on hollow sites of the surface and the calculated vibrational frequencies were in agreement with the experimental RAIRS spectra. Co-adsorbed oxygen produced a destabilization effect in the methoxy adsorption on the Ru(001) metallic surface. This method has been widely used to study adsorption processes yielding reliable results both on oxides and metal clusters. The C and O atomic orbitals were described with the all-electron 6–31G** basis set. For the inner and valence orbitals of Pd atoms, the effective core potential basis set LanL2DZ was used. Since the bare cluster models have close-shell ground states, spin-unpolarized calculations were performed. In the spin-polarized calculations for the positively charged and Cl modified clusters, the multiplicity with lower energy was 2. A 0.97 multiplying factor was used to scale the calculated frequencies

9

(chosen from the ratio of the theoretical value of the free CO stretching frequency and the gas-phase experimental value). The CO adsorption energies were corrected with the basis set superposition error (BSSE) via the standard counterpoise technique.

4. Results and Discussion

4.1. Hydrogen Chemisorptions and Particle Size Determination

The Pd catalysts characteristics are shown in Table I. The palladium particle diameter was calculated from H_2 chemisorption data using Equation (I), assuming semispherical particles and a density of surface atoms of 1.27×10^{19} Pd atoms $/m^2$ where D is the metal dispersion or the palladium-exposed fraction [35].

$$Dp[nm] = 1.12 / D \qquad \text{(I)}$$

Table I shows that a broad range of cluster sizes is obtained as a consequence of the metal precursors used and the metallic loading in each case. Palladium acetylacetonate ($Pd(C_5H_7O_2)_2$) links the metal to the surface by a ligand exchange method very specific to the octahedral site of the alumina support, generating small PdO clusters, which after reduction produces the metal particles [16]. It has been reported that Pd aggregates deposited with $Pd(NO_3)_2$ by the incipient wetness method produce larger Pd clusters [36]. Some authors reported dispersion values for a series of Pd-γ-Al_2O_3 supported catalysts using $Pd(C_5H_7O_2)_2$ as precursor [40]. There is an excellent agreement between the dispersion and particle size values for the A and B catalysts, and C and D samples when compared with the data obtained by Konopny et al. [16] for the catalysts reduced at higher temperatures where both suffer some sintering process. Good agreement was found in all the cases, verifying the H:Pd (1:1) ratio used for the chemisorption measurements.

10

The molar ratio of chlorine compound to Pd was 5:1 (Cl:Pd) to guarantee the Pd-Cl interaction. It is reported that chlorine is not completely eliminated from the catalyst surface by the oxidation and reduction treatment at high temperature [37]. These authors verified a partial chlorine elimination from the catalyst surface by flowing air or $Ar+H_2$ through the catalyst bed in a temperature ramp and bubbling this gas phase continuously in a vase containing an aqueous Ag solution. In the presence of chlorine AgCl precipitation occurs. In our case it is difficult to think that all the chlorine is eliminated after the calcination and reduction treatments, as was previously reported in Al_2O_3 supported catalysts [38]. In order to prove the chlorine presence, an amount of the support γ-Al_2O_3 was treated with 2-chloro-butane in the same way that the Pd catalysts. To determine the chlorine content, the procedure detailed in reference [39] was carried out. These authors slurred the sample in water and the hydrochloric acid resulting from the hydrolysis of the chlorine-containing catalysts is titrated potentiometrically with a standard base to pH=7. According to these authors all the chlorine from the catalyst is removed. The measured chlorine in the support correspond to a Cl:Pd ratio of 2.12. AgCl formation was observed after the pH measurement by the $AgNO_3$ addition. The dispersion values of this modified catalysts are showed in Table I, indicating a decrease in metal dispersion or more resistance to the metal reduction than the unmodified samples.

4.2. FTIR Studies

Figures 2 a), c) and e) show the FTIR spectra of CO adsorbed on A, B and C catalysts respectively exposed to 5 Torr of the gas. Their respective spectra after outgassing the samples are also presented. There are noticeable differences in the shape and intensity of the CO adsorption bands in A and B compared with those in the C catalyst, which shows a particular behavior. A deconvolution was made to the spectra, using different band centers

11

data according to the CO adsorbed species reported in the literature [41,42]. An

optimization was done with appropriate software reaching a $\chi^2<10^{-6}$ and Correlation

Coeficient >0.99 in all the cases. The area percentage and optimized band center of the

proposed species are summarized in Table II.

   The FTIR spectrum of CO on catalyst A (Figure 2 a)) shows bands corresponding to CO

on-top configuration (2070 cm^{-1}), and an asymmetric band attributed to isolated bridge

species shifted to lower frequencies (1900 cm^{-1}) that could include the three-fold CO type.

This result is in agreement with the high dispersion value found in chemisorption

measurements, indicating the presence of low coordination Pd aggregates. The band

corresponding to linear CO adsorption is intense and is shifted to a higher wavelength than

on Pd bulk, presenting some asymmetry. This band could be decomposed into two main

components: (2047 cm^{-1} and 2078 cm^{-1} see Table II) where the first one corresponds to CO

adsorbed on Pd with bulk properties [41]. The second one might be attributed to CO

vibration adsorbed on electron-deficient palladium ($Pd^{\delta+}$), since the observed band

frequency is between that of CO on Pd$^+$ and on Pd bulk. Tessier et al. [41] reported a

higher wavelength than that in our FTIR data, due to the fact that these authors recorded

their spectra with 100 Torr of CO pressure, where dipole-coupling interferes in C=O bond

vibration, displacing the position of the bands center to higher frequencies. Furthermore

Figure 2 a) shows a lower frequency band at 1590 cm^{-1}. In the present case, after

outgassing both bands move to lower frequencies, maintaining almost 52 and 110% of the

original band area, which expresses the strong C-metal bond of both CO species and also

an interconversion of linear to bridge type.

   The spectrum of CO adsorbed on the B catalyst (Figure 2 c)) presents an asymmetric CO

linear band at 2077 cm^{-1}, that could be decomposed into those two Pd species already

mentioned (2082 and 2052 cm^{-1} see Table II). The band at 1930 cm^{-1} corresponding to

bridge species shows a shoulder at 1980 cm^{-1} attributed to compressed CO bridge [44]. In agreement with the size increase, respect to A catalyst, the small amount of this configuration represents a diminutive fraction of developed planes. When the cell is evacuated, the linear and bridge bands decrease until 29 and 95% of the original ones persist adsorbed.

The spectrum of the C sample (Figure 2 e)) presents an intense band at 1990 cm^{-1}, which is not present in the case of catalyst A. This band was assigned to CO adsorption on more developed planes as might be expected on larger crystal size (as calculated from H_2 chemisorption). This band normally appears at 1990-2000 cm^{-1} in those catalysts prepared from $Pd(NO_3)_2$ where large cluster sizes are found and Pd(100) facets should be predominant, allowing numerous CO neighbors to be coupled [41,45]. The spectrum shows that the bridge band is wider than in the A and B catalysts, evidencing that isolated bridge and three-fold bridge CO configurations have many different energetic sites for adsorption in agreement with reference [41]. The low signal is characteristic of the precursor used and the low dispersions obtained. After outgassing the sample, the entire linear band disappears and less than 26% of the bridge species remains adsorbed. A band at 1660 cm^{-1} also appears similar to that observed in Figure 2 a) for the A catalyst. This band was attributed to several CO_3^- species on Al_2O_3, evidence of some CO disproportion from the shift reaction that involves the support humidity [43]

Table II shows that the area percentage of the linear CO species is 42.1, 17.6 and 14.1% for A, B and C catalysts respectively. The contributions of CO adsorption on $Pd^{\delta+}$ are 14.7, 8.0 and 0% in each case of the series. The CO isolated bridge and the compressed bridge species increase their percentage area from 23.2 to 46.5% and from 0 to 9.5 % respectively when the exposed metal area decreases. These bands were assigned to Pd (110) and Pd(100) planes respectively [45,46].

The shift to a higher frequencies of the linear band observed for A and B samples (Figure 2 a) and b)) was previously reported [17,18,53] and was attributed to an electronic effect on Pd due to charge transfer from the metal to O atoms in Al_2O_3. The latter is evidenced by the lower retro donation of d electrons of the metal to the π anti-bonding orbital of the carbon in the CO molecule directly influencing the vibrating energy of the C=O bond. In these cases we suppose that there is no interference in the band displacements caused by the CO dipole-dipole coupling, because the CO pressure in the IR cell is low (5 Torr). Anderson referred to the fact that particles smaller than 2 nm are electron deficient and the Pd atoms change the metallic character due to the interaction with the support [36].

In order to test this hypothesis an electron acceptor (such as chlorine) was added to our set of catalysts. Figures2 b), d) and f) show the FTIR spectra of CO adsorbed on these modified catalysts, and Table III summarizes their respective spectra deconvolution results.

In the A+Cl catalyst, the absorption band corresponding to linear CO type is also shifted to higher wavelengths (2080 cm^{-1}) and the spectrum is similar to that of the unmodified sample but an intense band appears at 1650 cm^{-1} attributed to carbonates on Al_2O_3. When this catalyst was outgassed, 46 and 96% of the linear and bridge species remained at the surface. In the spectrum of CO on B+Cl (Figure 2 d)), the main band of the bridged CO is shifted (20cm^{-1}) to higher frequencies compared with the spectrum corresponding to B catalyst. The shoulder at 1980 cm^{-1} attributed to compressed bridge CO is almost undistinguished because this band does not suffer displacements due to the strong CO coupling effect [41], and the CO isolated bridge band overlaps it. The outgassed catalyst spectrum shows that 25% and 96% of the linear and bridge species remain adsorbed. The latter shifts from 1950 to 1910 cm^{-1}. The band at lower assigned to carbonate formation appears again.

When the C+Cl catalyst was reduced under the same conditions as those of the

unmodified catalyst (373 K, 1h under 700 Torr of H_2), its spectrum (not shown in the

Figure 2) presented bands at 2170 and 2120 cm^{-1} attributed to CO adsorbed on cationic Pd

species (+1 and +2 respectively) probably combined with chlorine [41]. It is reported that

the chlorine-modified catalysts are difficult to reduce. This effect is attributed to an

electronic effect upon the metal [53]. The FTIR spectrum of the C+Cl catalyst reduced at

473K after 2 h and 700 Torr of H_2 is shown in Figure 2 f). The linear CO absorption is

more intense relative to C sample and is displaced up to 2070 cm^{-1}. Also it presents the

same asymmetry as that in A+Cl and B+Cl spectra, and then CO adsorption on $Pd^{\delta+}$ occurs

in this case too. Furthermore a single band of bridged species is observed (1940 cm^{-1}) in

the frequency range of the isolate bridge CO, shifted $20cm^{-1}$ to higher wavelengths

compared to the same in the C spectrum. This is narrower than on the unmodified catalyst

and could include three-fold bridge species. In Figure 2 f) the band corresponding to

compressed bridge CO species, absorbing between 1970-1990 cm^{-1}, is absent probably due

to the blocking effect caused by the bulky Cl atoms adsorbed in the most developed facets.

This obstruction does not allow the multiply coordinated CO adsorption on Pd (100) plane

to be achieved. Furthermore significant dispersion of the data is observed around 1650 cm^{-1}, attributed to excessive signal noise in the background influencing the observation of the

CO_3^- on Al_2O_3 band. Evacuating the sample, 27% of the linear CO and 73% of the bridge

species are maintained on the surface. This phenomenon was remarkably higher than in the

case of the C catalyst.

Table III shows that CO adsorbed on $Pd^{\delta+}$ is the main component of the linear species for

all the catalysts. The isolated bridge configuration increases its relative amount in the total

bridge type for all the catalysts relative to the unmodified samples. The C+Cl catalyst

presents a more interesting change: the linear CO absorption area is increased almost twice

more than in the C sample and CO adsorbed on $Pd^{\delta+}$ is 39.8% of the total on-top type. The isolated bridge and the three-fold CO species are 29% larger and 59% smaller respectively than the same configuration adsorbed on C sample.

4.3. DFT Results

In order to test the hypothesis related to electron deficient Pd ensembles; a theoretical study of CO adsorption was performed based on the Density Functional Theory. The calculations were carried out for Pd_{19} and Pd_{13} cluster models, adsorbing CO on one-fold (on-top) and two-fold (bridged) sites. Calculations for electron deficient Pd clusters were also performed. By extracting an electron charge from the whole cluster an electronic deficiency was generated in both models (Pd_{19}^{1+} y Pd_{13}^{1+}). Besides, the behavior of chlorine-modified Pd particles was studied. For that purpose, the Cl atom was placed on a two fold site, which is the more favorable configuration for Cl adsorbed on Pd. All the adsorption properties are summarized in the Table IV and the final geometries of the molecules are shown in Figure 3.

For the on-top CO configuration, the C-O stretching frequencies are the same on both neutral Pd_{13} and Pd_{19} clusters, but higher energy stability (difference of 0.29 eV) is achieved for the small particle. This result is in agreement with the larger amount of on-top CO retained on the A catalyst after outgassing. When the positively charged clusters are considered, the stabilization is different for Pd_{13} than for Pd_{19} particles. The CO molecule on the latter has the same stability as on the neutral cluster. However, on a Pd_{13}^{+} particle the CO adsorption is destabilized. This indicates that certain repulsion is present for the CO molecule adsorbed on charged Pd_{13} clusters. In both cases, the C-O vibrational frequency increases with respect to the neutral clusters (blue shift of 30 and 60 cm^{-1}, for Pd_{19}^{+} and Pd_{13}^{+}, respectively), in agreement with the IR bands reported for A and B catalysts in Table

II. The Pd-C and C-O distances go in opposite ways when the charged and not charged clusters are considered. The lower back-donation from d metal orbitals to the unoccupied π^* level of CO, due to the removed electron from the metal particles, produces an enlargement of the Pd-C bond and a reduction of the C-O bond, with respect to the unmodified cluster.

When a Cl atom is added to a Pd_{13} particle, 0.2 eV nearly stabilizes the CO molecule with respect to the neutral Pd_{13} particle. This result is in line with the A+Cl catalyst FTIR results, where the proportion of CO adsorbed on $Pd^{\delta+}$ atoms is higher than on catalyst A (27% vs. 14.7%). On the other hand, the frequency changes in the same direction as the positive charged particle, giving a frequency of 2070 cm^{-1}, compatible with a higher oxidation state of the Pd atom. From this 40 cm^{-1} shift to a higher wavelength, it is possible to infer that the withdrawing effect of the Cl atom in a small particle cluster is lower than that obtained for a positively charged model. This result indicates that an electron deficient small particle could not be greatly modified by the addition of a Cl atom (shown in the FTIR spectra of Fig 2a) and 2b)). Notice that the IR data based on the mean band positions indicate negligible shifts due to Cl; nevertheless, blue shifts of nearly 10 cm^{-1}, can be observed on the peaks for on-top CO.

The CO on-top configuration adsorbed on a Cl modified Pd_{19} cluster was not reported because the CO molecule takes a hollow geometry as a more stable configuration. This on-top destabilization can be attributed to a steric impediment produced by the Cl atom near the CO molecule.

In bridge CO configuration, the adsorption energies difference between Pd_{13} and Pd_{19} neutral clusters is larger, again favoring the adsorption on small particles by 0.7 eV. These results are in agreement with the lager amounts of CO bridge type retained after evacuation on A and B catalysts, with respect to C catalyst. The CO stretching frequencies

calculated for bridge configuration on both Pd clusters are smaller than those experimentally obtained for A to C catalysts (1900-1980 cm^{-1}). Nevertheless, in the open literature, some experimental data reported IR bands located from 1880 to 1950 cm^{-1} [47]. On the other hand, the stretching frequency dependence of CO surface coverage on Pd(111) studied by means of the periodic density-functional theory showed a good agreement with our results for CO adsorbed in bridge configuration at a coverage of 0.33 ML [48].

The CO two-fold adsorption on the Pd_{13}^{+} was less stable in comparison with the neutral Pd_{13} particle. The destabilization was smaller than that for the CO on-top configuration (0.08 eV and 0.25 eV, respectively). The last observation is in agreement with the amount of CO retained in A and B catalysts after outgassing; indeed, the CO on-top band decreases more significantly than the CO bridge band. Taking into account the adsorption energy change observed on the positively charged Pd_{13} cluster for both geometrical configurations, we conclude that extracting an electron from this cluster produces a destabilizing effect [49]. The C-O stretching frequency increases likewise in the case of CO on-top ($\Delta\omega$= 47 cm^{-1}), indicating a higher oxidation state for the metal atom. On the other hand, the addition of Cl on the Pd_{13} cluster yields a stabilization of 0.22 eV. The absorption band is shifted to a higher wavelength ($\Delta\omega$= 10 cm^{-1}). This displacement is less pronounced than that produced by the positive charged particle.

For the Pd_{19}^{+} cluster, the CO species adsorbed in bridge configuration is more stable than the case adsorbed on the neutral particle (0.19 eV). The CO stretching frequency shows a blue-shift of 58 cm^{-1}. The addition of chlorine onto the Pd_{19} cluster gives almost the same results as on the charged particle. On the other hand, the IR data shows that the C+Cl catalyst has a higher retention of the CO bridge type, in comparison with the C

catalyst. Taking into account the previous comments, we conclude that a positive charged Pd_{19} model, as well as the chemically modified Pd_{19} model, could simulate this behavior.

Electron density difference maps can provide the charge redistribution, when cluster models with electronic differences interact with the CO molecule. The electron density gain of these clusters is visualized as the solid lines on the Pd atoms and on the adsorbed Cl atom. Figure 4 shows the mode CO top adsorption only on the three different electronic Pd_{13} clusters. Comparing the results of Pd_{13}^{+} with Pd_{13}, we notice for the former, less extended lobules on the O atom of CO and small charge accumulation in the region between the C and Pd atoms. In the $Pd_{13}Cl$ particle, these effects are less pronounced giving an intermediate situation between the unmodified and the charged cluster.

In almost all the cases, the adsorption on small particles is stronger and produces a band shift to higher frequencies, in agreement with the experimental FTIR results. Particles with a lower electron density such as the small clusters could adsorb a Lewis base as CO more strongly than larger particles having bulk-like properties. The chlorine modification shows a stabilization of the linear and bridge CO species increasing their adsorption energies.

4.4. Catalytic Tests

A generalized criterion, the Weizs-Prater modulus[50] was used to determine the mass transport limitations inside the pore structure of the catalysts, considering spherical catalyst particles with a ratio volume/external surface equal to $D_p/6$. In the modulus equation *(-r_{OBSi})* is the apparent consumption rate of the i reactant. This dimensionless number evaluates the concentration gradient between the external surface and the inside of the pore structure. If the Φ modulus of the *i* reactant is <0.03 there are no mass transfer limitations and the concentration difference is lower than 5%. If $\Phi_i>0.7$ the mass transfer limitation is serious and is controlling the global rate.

$$\Phi_i = \frac{(-r_{OBSi})\rho_{cat}D_p^2}{36D_{effi}C_i} \qquad (I)$$

The Φ_i values are presented in Table V assuming $D_{eff}\,H_2 = 1\ 10^{-7}\,m^2\,s^{-1}$, $D_{eff}\,TG = 1\ 10^{-9}$ $m^2\,s^{-1}$ [52], $C_{H2} = 947.8\,mol\,m^{-3}$, $C_{TG} = 321.5\,mol\,m^{-3}$, $\rho_{cat} = 3750\ kg\,m^{-3}$ and support particle diameter, Dp $= 74\ \mu m$. For the reaction carried out at the same Pd/Triglyceride ratio (wt/wt %), Table V shows that H_2 is free of mass transport problems, although Φ values for triglyceride molecules remain above the lower limit ($0.03 < \Phi_{TG} < 0.7$). Such Φ_{TG} values, neart to the lower border, indicate that mass transport does not obstruct the global catalyst behavior. These results suggest a scenario where the catalyst surface is saturated with hydrogen while the triglyceride should be in a lower proportion. This situation was reported by other authors for the same system ($H_2 + C_3H_8 + TG$) [9,59].

Table V also shows that smaller particle sizes have less specific activity than larger ones. This effect is attributed by some authors to the strong adsorption of high-unsaturated chains present in the fatty acids as happens for lighter di-alquenes and acetylenic compounds [17,61]. They proposed the electronic modification of the small Pd clusters due to the strong interaction with the oxygen of the alumina [53]. The chlorine modification reduces the specific activity by 30% for B catalysts and 42% for C catalysts, but in the case of A catalysts the activity remains almost at the same level. In the first two cases the chlorine inhibition should be interpreted as an esteric effect over the adsorption sites, blocking them, or as a partial poisoning due to an electronic effect. It was reported that chlorine combines with the Pd atoms and alters their adsorption properties [54]. Some authors using XPS technique, informed increments of 0.9 eV of the Pd $3d_{5/2}$ energy band for 1% Pd/γ-Al$_2$O$_3$ $(150m^2g^{-1})$ prepared from PdCl$_2$ in HCl solution, [53]. The A+Cl catalyst activity could be explained by the adsorption of chlorine on Al$_2$O$_3$ rather than on Pd. The intense carbonate band observed in the FTIR spectra is an indication of this (see

Figure 2 b)). The CO molecules found more acid sites in the support after chlorine addition.

On the same lines as the activity results, the metallic particle size and the chlorine modification also influence the product distribution. In both cases the selectivity changes, a decrease in the isomerization (*trans* isomers) and an increase in the saturated fatty acid content occur during the reaction [2]. The A and B samples produce 28% more saturates than the C catalyst (see Table V). At the same time, *trans* isomers for the A and B catalyst reactions decrease 35% approximately compared with C and D. A similar difference is produced when the C+Cl catalyst is compared with the same catalyst without chlorine addition. Similar selectivity modification was reported earlier in the methyl ester fatty acids hydrogenation, utilizing a Pd(1%)-C catalyst, when the mass transport condition was varied by adjusting the catalyst pore size [55]. These authors informed that by decreasing the triglyceride mass transport the concentration of polyunsaturated compound is much lower than the corresponding equilibrium values, favoring the direct hydrogenation of the diunsaturated fatty acid to the completely saturated one ("shunt" reaction) and obtaining a greater amount of saturated compounds than those normally produced. Other authors proposed a similar conclusion since they could not adjust their kinetic model properly without considering a shortcut pathway between diene to saturate fatty acids esters [56,57]. In the selective hydrogenation of polyunsaturated fatty acids, hardly any monounsaturated fatty acid is hydrogenated at the beginning of the reaction. This phenomenon is explained assuming that polyunsaturated compounds are more strongly adsorbed on the catalyst surface than the monounsaturated fatty acids [2,57]. On the other hand, *trans* isomers are rapidly formed by a side reaction on the catalyst surface during the hydrogenation of *cis*-monoene [3]. In a previous work [15] we compared part of our results against those obtained by other authors for the same reactive system in a homogeneous phase condition

[59]. We concluded that in spite of the better mass transport conditions found for the triglyceride molecule, the saturated content was considerably higher (64%) than the value belonging to the reference work. This difference was attributed to some catalyst property. Some authors proposed the shunt pathway in amounts between 15 to 25% of the consecutive reaction to properly fit their experimental data [60]. They tested Pd, Pt and Ni catalysts and found that the shortcut alleyway might most likely be attributed to a diffusion effect. But its independence of the temperature, the viscosity of the liquid and catalysts support properties, suggest that some other factor is responsible. In this way, we concluded that Pd electronic state was responsible for this modification, as was earlier reported in the literature for the 1-3 butadiene hydrogenation [17,18]. These authors studied the hydrogenation over Pd, Pt y Rh alumina supported catalysts with dispersion from 9 to 100%. They modified the same catalysts with electron acceptors and donor compounds such as terc-butylchloride and piperidine respectively. The addition of modifiers to small particles altered the *d* electrons state of Pd atoms, changing the specific activity and raising the consumption of the monounsaturated compounds (1 y 2-butenes) as well as the direct hydrogenation of diene to saturated alkanes. In this way, the electronic effect upon Pd promotes the augmentation of butane concentration, diminishing the consecutive hydrogenation and the 1 and 2-butenes compounds as well as the *trans/cis* ratio. A similar effect but in the opposite direction, was observed for the piperidine addition which enhanced the metallic character of the Pd particle. In this case these authors attributed the selectivity difference to the possible presence of electron deficient particles which could reinforce the Pd-C bond and in this way increase the possibility of forming of multi-bonded intermediates. Others observed displacements of 0.7 eV higher than the bulk energies of Pd $3d_{5/2}$ for 1.9% Pd supported on γ-Al$_2$O$_3$ (200m^{2}g^{-1}) utilizing Pd(C$_5$H$_7$O$_2$)$_2$ as metal

precursor [61]. These authors arrived at equal selectivity performance for small metal particle sizes (<4nm) in the hydrogenation of vinylacetylene.

An identical trend in activity and selectivity was found in this work, diminishing the isomerization products and increasing the production of saturated compounds when catalysts modified with chlorine or with small cluster sizes were used. The shifts to higher wavelengths of the FTIR bands of CO adsorption for A, B and C+Cl catalysts could be explained by less retrodonation of the *d* electrons of Pd atoms due to the electron density depression caused by interaction of this band with the O of the alumina support or by chlorine atoms adsorbed in a bridge configuration on Pd, as demonstrated by the theoretical calculations and reported in the literature [53]. The C catalyst exhibits the most interesting change in the activity and selectivity results due to chlorine addition. In this case the isomerization products diminish 39% compared to the same catalyst without modification, where both reactants are free of mass transport limitation (see Table IV). The A+Cl catalyst presents a less modified product distribution, contrary to that reported by Botiaux et al.[18]. This could be explained by assuming that the added chlorine does not strongly interact with Pd and that the O atoms of the support could affect *d* electrons of the active metal in agreement with theoretical results. When the particle size increases, the metallic character of Pd in contact with the reactive is unaltered by the interaction with the alumina, but it could be changed by a modifier addition, like in the case of the C+Cl catalyst.

As mentioned above, the strong adsorption of polyunsaturated fatty acid chains of triglyceride molecules promotes their hydrogenation in the first place [2,4,57]. The shortcut reaction from linoleic to saturated fatty acids depends exclusively on the simultaneous double bond adsorption and their adsorption energy [57], influenced by the *d* electrons density of the exposed Pd atoms. The electron deficiency makes the cluster strongly adsorb a Lewis base as a double bond and retaining it on the metal surface until a H atom is added

to the C of the hydrocarbon chain. In this way the probability of the hydrogenation pathway is raised. The retention at the surface of the CO bridge species after the evacuation, as well as the theoretical calculation (see Table IV), demonstrates the greater adsorption strength on Pd electron deficient particles (A and B as well as in C+Cl catalysts) compared to Pd with bulk-like properties (C and D catalysts). These results, together with the lower isomers production and the decrease in specific activity, bring us to suppose that the shortcut pathway is favored in these catalysts with developed planes (Pd(110) and Pd(111)) with lower electronic density. The bridge species strongly adsorbed on them should play a key role. It is reported that Pd(110) plane promotes the di-σ adsorption of lighter diolefins and Pd(111) promotes the three-fold CO adsorption in hollow sites. The direct hydrogenation pathway of acetylenic compounds was attributed to this last one [62]. On the other hand the selectivity difference of the 1,3-butadiene hydrogenation, in which the bridge species adsorbed on Pd(111) and Pt(111) are the intermediates, was attributed to the adsorption energy variation between both metals [63]. It seems that the key to the selectivity of saturated fatty acids lies in the relative stabilities of radical intermediates on Pd(110) and Pd(111). On the electron deficient palladium surface, the formation of radical species seems to compete with the monounsaturated fatty acids chains desorption. This could explain its poor selectivity to monoenes and the formation of saturated chains as a primary product.

5. Conclusions

Triglyceride hydrogenations carried out in single-phase conditions are free of mass transport limitations for H_2 and high molecular weight substrate. Under these conditions the reaction activity and selectivity exhibits some change with the metal surface morphology. TOF values and saturated fatty acids differences were found when the

reaction was tested with catalysts of different metal particle size (from 1,1 to 12,1 nm) and with the same catalysts modified with chlorine. The catalysts with small metal particles, as well as those modified with chlorine, produce lower amount of isomerization products with a parallel increase of saturated fatty acid chains. These results are explained by a modification of the electronic properties of the Pd clusters, which modifies their adsorption properties. The lower electronic density of the Pd particles was sensed by the band displacement of the FTIR adsorption bands of CO and explained by DFT calculations and could be due to the interaction of the metal with the O of the alumina support or with the Cl adsorbed on it. In this calculation the electron deficiency and Cl modification was proposed for two Pd clusters in which the lower metallic character stabilizes the C-metal bond (di-σ or π intermediaries) favoring the retention on the surface of the hydrocarbon chain. In this way a shortcut pathway from diunsaturated to saturated fatty acid chains ("shunt" reaction) is enhanced. This alleyway could be favored by Pd(111) and Pd(110) planes of electron deficient clusters.

6. Acknowledgements

References

[1]   B. Fillion; B. Morsi; K. Heier; R. Machado, Ind. Eng. Chem. Res. 41 (2002) 697.

[2]   J.W. E. Coenen, Ind. Eng. Chem. Fundam. 25 (1986) 43.

[3]   I. Horiuti, M. Polanyi, Trans. Faraday Soc. 30 (1934) 1164.

[4]   H.B. Patterson, Hydrogenation of of Fats and Oils: Theory and Practice, second ed., J. AM. OIL CHEM. SOC. Press, Illinois, 1994, pp 1-28.

[5]   R. Mensink, M. Katan, N. Engl. J. Med. 45, (1990), 323.

[6]   C. Chou, Inform 17 (2006) 528.

[7]   A. Baiker, Chem. Rev. 99, (1999), 453.

[8]   M. Macher, J.Högberg, P. Møller, M. Härröd, Lipid – Fett. 8 (1999) 301.

[9]   M. Macher, Supercritical Hydrogenation of Vegetable Oils, Ph.D. Thesis   Chalmers University of Technology, Göteborg, Sweden 2001.

[10] M. Hitzler, F. Smail, S. Ross, M. Poliakoff, Org. Proc. Res. Dev. 2 (1998) 137–146.

[11] R.Wandeler, N. Künzle, M.S. Schneider, T. Mallat, A. Baiker, J. Catal. 200 (2000) 377–388.

[12] M. Burk, S. Feng, M. Gross, W. Tumas, J. Am. Chem. Soc. 117 (1995) 8277–8278.

[13] B. Bhanage, Y. Ikushima, M Shirai, M. Arai, Catal. Lett. 62 (1999) 175–177.

[14] S. van den Hark, M. Härröd, App. Catal. A: General 210 (2001) 207–215.

[15] C. Piqueras, S. Bottini, D. Damiani, App. Catal. A: General 313 (2006) 177–188.

[16] L. W Konopny, "Preparación, Caracterización y Ensayo de Catalizadores de Pd-Mo Soportados en Gamma Alumina", Ph.D. Thesis Universidad Nacional del Sur , Bahía Blanca, Argentina 1996.

[17] J. Botiaux, J. Cosyns, E. Robert, Appl. Catal. 49 (1989) 219.

[18] J. Botiaux, J. Cosyns, E. Robert, Appl. Catal. 49 (1989) 235.

[19] A. Pisanu, C. Gigola, Appl. Catal. B 11, (1996), 37.

[20] J. Benson, H. Hwang, M. Boudart, J. Catal. 30, (1973), 146.

[21] S.J Chen., R. E. Randelman, R. L. Seldomridge, M. Radosz, J. Chem. Eng. Data 38, (1993), 211.

[22] L. Rovetto, S. Bottini, E. Brignole, J. Supercrit Fluids 25, (2003), 165.

[23] E. Straver, J. de Roo, C. Peters, J. de Swaan Arons, (1994), Supercritical Engineering Science: Fundamentals and Applications, ACS Symposim Series, (Eds.) E. Kiran, J. Brennecke, p 46.

[24] S. Pereda, S. Bottini, E. Brignole, AIChE J. 48, (2002), 2635.

[25] I.V. Yudanov, R. Sahnoun, K.M. Neyman, N. Rösch, J. Chem. Phys.117 (2002) 9887.

[26] F. Illas, S. Zurita, A.M. Márquez, J. Rubio, Surf. Sci. 376 (1997) 279.

[27] F. Illas, N. López, J.M. Ricart, A. Clotet, J.C. Conesa, M. Fernández-García, J. Phys. Chem. B 102 (1998) 8017.

[28] M. Neurock, R.A. van Santen, J. Phys. Chem. B 104 (2000) 11127.

[29] A. D. Becke, J. Chem. Phys. 98 (1993) 5648.

[30] M.J. Frisch, y col., Gaussian 03, Revision C.02, Gaussian, Inc., Pittsburgh PA, 2003.

[31] [5] T. Bredow, G. Pacchioni, Chem. Phys. Letters 355 (2002) 417.

[32] M.M. Branda, P.G. Belelli, R.M. Ferullo, N.J. Castellani. Catal. Today 85 (2003) 153.

[33] T. Vazhappilly, S. Beyvers, T. Klamroth, M. Luppi, P. Saalfrank, Chem. Phys. 338 (2007) 299.

[34] M.N.D.S. Cordeiro, A.S.S. Pinto, J.A.N.F. Gomes, Surf. Sci. 601 (2007) 2473.

[35] P. Aben, J. Catal. 10 (1968) 224.

[36] J.R. Anderson, Structure of Metallic Catalyst (1975), Academic Press, New York.

[37] T. Narita, H. Miura, K. Sugishama, T. Matsuda, R. Gonzalez, J Catal 103 (1987) 492.

[38] F. Stoop, A. Verbiest, K. van der Wiele, Appl. Catal. 25 (1986) 51.

[39] J.P. Giannetti, R.T. Sebulsky, Ing. Eng. Chem. Res. Dev. 8 (1969) 356.

[40] J. Botiaux, J. Cosyns, S. Vasudevan, Appl. Catal. 6 (1983) 41.

[41] D. Tessier, A.Rakai, F. Bonzon-Verduraz, J. Chem. Soc. Faraday Trans. 88, (1992), 741.

[42] M. Primet, J. Basset, M. Mathieu, M. Prettre, J. Catal. 29, (1973), 213.

[43] K. Foger, J. Anderson, App. Surf. Sci. 66 (1977) 101.

[44] R. Hicks, H. Qi, A. Kooh, L. Fischel, J. Catal. 124 (1990) 488.

[45] A. Ortega, A. Hoffman, A. Bradshaw, Surf. Sci. 119 (1982) 79.

[46] G. Ertl, P. Rau, Surf. Sci. 15 (1969) 443.

[47] A. Eichler, J. Hafner, Phys. Rev. B 57 (1998) 10110 .

[48] D. Loffreda, D. Simon, P. Sautet, Surf. Sci. 425 (1999) 68.

[49] A.M Ferrari, K.M. Neyman, T. Belling, M. Mayer, N. Rösch, J. Phys. Chem B, 103 (1999) 216.

[50] P. B. Weisz and C. D. Prater, Adv. Catal. 6 (1954) 143.

[51] K. Westerterp, W. van Swaaij, A. Beenackers, Chemical Reactor Design and Operation, 2nd ed., Jhon Wiley Sons, New York, 1984, pp 448-451.

[52] K. Liong, P. Wells, N.Foster, Ind. Eng. Chem. Res. 31, (1992), 390.

[53] E. Cunha, F. Faccin, C. Moro, E. Benvenutti, Quim. Nova 25 (2002) 392-395.

[54] P. Marécot, A. Fakche, B. Kellari, G. Mabilion, M. Prigent, J. Barbier, Appl. Catal. B: Envirom. 3 (1994) 283.

[55] K. Tsuto, P. Harriott, K. Bischoff, Ind. Eng. Chem. Fundam., 17(1978) 199.

[56] R. Grau, A Cassano, M Baltanás, J. Am. Oil Chem. Soc. 67, (1990), 226.

[57] I. Heertje, G. Koch, W. Wösten, J. Catal 32 (1974) 337.

[58] J. Lidefelt, J. Am. Oil Chem. Soc. 60 (1983) 593.

[59] E. Ramírez, F. Recasens, M. Fernández, M. Larrayoz, AIChE J. 50, (2004), 1545.

[60] C. Scholfield, R. Butterfield, H. Dutton, J. Am. Oil Chem. Soc. 49 (1972) 586.

[61] Y. Ryndin, L. Nosova, A. Boronin, A. Chuvilin, App. Catal, 42 (1988) 131-141.

[62] H. Molero, B. Bartlett, W. Tysoe, J. Catal 181 (1999) 49.

[63] A. Valcarcel Ortí, "Modelling unsaturated hydrocarbons on metals: towards understanding catalytic processes", Univaersitat Rovira I Virgili, Cataluña, Spain, 2007.

Table I. Metallic content, dispersion and average Pd particle size for A, B and C catalysts as well as for the chloride modified samples. *See reference [29]. #Data referred from [18], for similar metallic charge. Comparisons of the values of A and B reduced at 573 K and 973 K for C and D catalysts.

Table II. Band Centers and Area Percent for A, B and C catalysts, results of the deconvolution. The initial location of the band maximum was tacked from reference [30].

Table III. Band Center and Area Percent for A, B and C catalysts modified with Cl results of the deconvolution. The initial location of the band center was tacked from reference [33]. Two bands at 2117 and 2171 cm^{-1} appears in the unreduced sample and could be assigned to CO on top adsorbed on Pd^+ and Pd^{+2} (the areas of the cationic palladium are 5.5 and 6.8% respectively).). # This band could be composed by two main band 1920 and 1951 cm^{-1} both in the isolated bridge with 31.4 and 13% area percentage.

Table IV. Metal-Atom distances, Adsorption Energies and calculated wavelength (υ) from DFT model. *The Cl and CO position in bridge configuration was changed to check the boundary influence. Geometric differences lower than 0.01Å was founded, verifying no boundary interference.

Table V. Activity and selectivity values for the set of unmodified and Cl modified catalysts. TOF and Weisz-Prater modulus values were calculated for rate values at x_{H2}=5%. The *trans* and saturated fatty acid content were tacked at x_{H2}=50%.

Table I

Catalysts	A	B	C	D
Metal %	0.33	0.78	0.77	0.77
Dispersion	0.95	0.6	0.29	0.09
Dp [nm]	1.1	1.9	3.9	12.4
Catalysts	**A+Cl**	**B+Cl**	**C+Cl**	**-**
Dispersion	0.86	0.53	0.20	-
Dp [nm]	1.3	2.1	5.6	-
Metal %	0.33*	0.76*	0.76[#]	0.9[#]
Dispersion	1	0.6	0.27	0.04
Dp [nm]	0.4	1.1	3.2	30

Table II

CO specie	Band center [cm^{-1}]			Area [%]		
	A	B	C	A	B	C
	$\chi^2\ 10^6$			R^2		
	11	3.1	0.59	0.992	0.996	0.993
CO three-fold bridge	1861	1892	1828	34.7	39.9	29.9
CO isolated bridge	1940	1946	1937	23.2	36.5	46.5
CO compressed bridge	-	1978	1987	0.0	6.0	9.5
CO on top on Pd^0	2047	2052	2057	27.4	9.6	14.1
CO on top on Pd$^{\delta+}$	2078	2082	-	14.7	8.0	0.0

Table III

CO specie	Band center [cm^{-1}]			Area [%]		
	A	B	C*	A	B	C*
	$\chi^2\ 10^6$			R^2		
	18	2.4	0.51	0.992	0.995	0.990
CO three-fold bridge	1865	1875	1879	17.8	28.8	12.3
CO isolated bridge	1917	1945	1936[#]	33.2	49.9	60.0
CO compressed bridge	-	1979	-	0.0	0.4	0.0
CO on top on Pd^0	2048	2044	2055	22.0	9.0	16.6
CO on top on Pd$^{\delta+}$	2079	2078	2083	27.0	11.0	11.1

Table IV

CO	Model	Optimized Distances [Å]			E_{ads} [eV]	ν [cm^{-1}]
		Pd-C	C=O	Pd-Cl		
On-Top	Pd$_{13}$	1.909	1.151		-1.23	2033
	Pd$_{13}^{1+}$	1.938	1.143		-0.98	2091
	Pd$_{13}$-Cl$_{brid}$	1.911	1.146	2.452	-1.42	2070
	Pd$_{19}$	1.891	1.150		-0.94	2033
	Pd$_{19}^{1+}$	1.919	1.146		-0.96	2060
Bridge	Pd$_{19}$	1.983	1.175		-0.95	1831
	Pd$_{19}^{1+}$	2.018	1.168		-1.14	1889
	Pd$_{19}$-Cl$_{brid}$*	1.993	1.168	2.540	-1.17	1885/ 1889
	Pd$_{13}$	2.036	1.172		-1.65	1875
	Pd$_{13}^{1+}$	2.033	1.164		-1.57	1922
	Pd$_{13}$-Cl$_{brid}$	1.980	1.171	2.447	-1.87	1885

Table V

Catayst	TOF [s^{-1}]	Φ_{H2}	Φ_{TG}	*Trans* [%]	Saturated [%]
A	12.2	0.006	0.100	19.1	27.5
B	16.1	0.004	0.073	20.3	29.4
C	20.3	0.003	0.049	32.5	20.6
D	31.9	0.002	0.027	31.8	18.4
A+Cl	11.9	0.006	0.107	16.5	31.1
B+Cl	11.3	0.003	0.056	17.0	36.5
C+Cl	18.7	0.003	0.053	19.7	32.9

Figure 1. a) Pd19 Cluster (12:7) d(Pd-Pd)= 2.751 Å (Pd bulk distance), d(Pd-Pd)central= 2.52 Å, b) Spherical Pd13 Cluster; d(Pd-Pd)= 2.84 Å (optimized).

Figure 2. FTIR of CO adsorption on Pd catalysts at 324 K. Black line: 5 Torr CO, gray line: Outgassed sample. a) catalyst A b) A+Cl. c) catalyst B d) B+Cl. e) catalyst C f) C+Cl. Each spectrum was decomposed into gaussians bands with $\chi^2 < 2.10^{-6}$. To the deconvolution five peaks was proposed, corresponding to the species: (1890-1850 cm^{-1}) CO bridged three-coordinated, (1925-1960 cm^{-1}) CO bridged isolated, (1975-1995 cm^{-1}) CO bridged compressed, (2050-2100 cm^{-1}) CO lineal. The bands at (2117-2170 cm^{-1}) are attributed to CO on Pd^+ and Pd^{+2} respectively [33]. The number showed corresponding to the experimental main bands. The lower CO signal of the C catalysts was attributed to the precursor used.

Figure 3. Final disposition of CO and Cl, on Pd13: a) CO on top b) CO bridge c) CO on top and Cl bridge d) CO and Cl bridge. Final disposition of CO and Cl, on Pd_{19} cluster both CO and Cl were confined to the adsorption on the first layer to get to calculus stability: e) CO on top f) CO bridge g) CO on top and Cl bridge f) CO and Cl in bridge were exchanged to corroborate if boundary interfere with the results.

Figure 4. Electron density difference maps for CO top adsorption mode on: (a) neutral Pd13, b) Pd13+ and c) Pd13Cl clusters. Solid and dashed lines indicate positive and negative values, respectively. The contours are drawn at ±1.0, ±0.5, ±0.25, ±0.125, ±0.0625, …, ±0.000488 au.

a)   b)
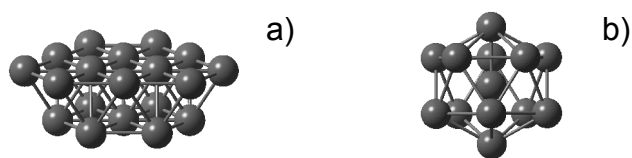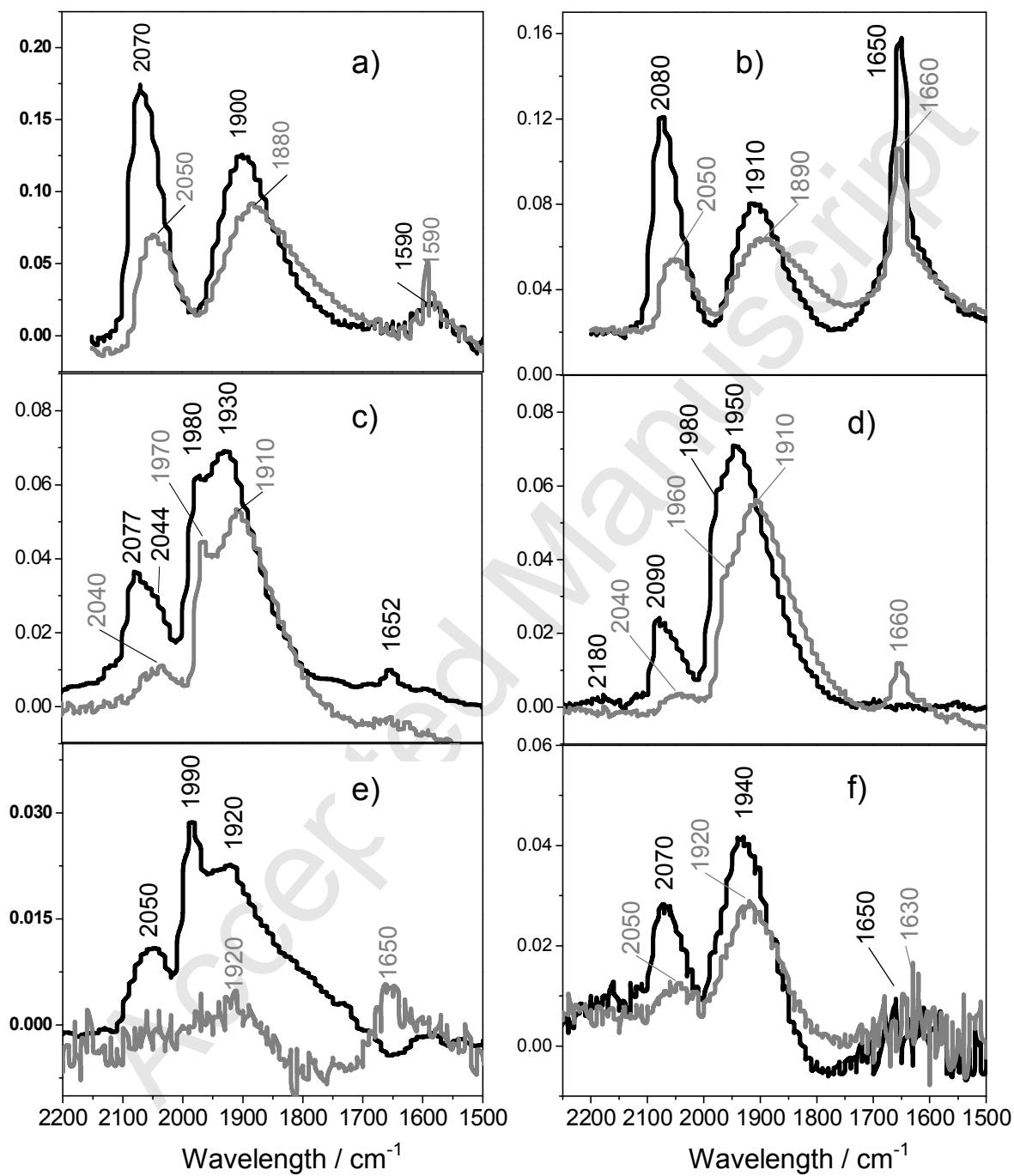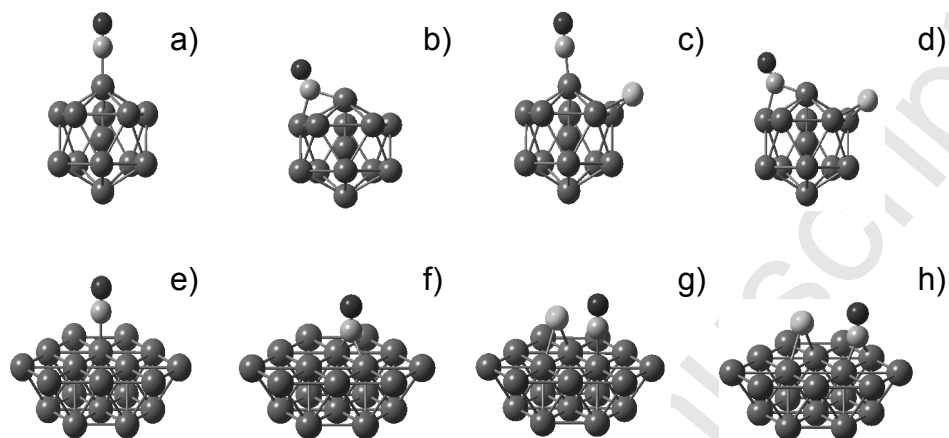
Figure 1.
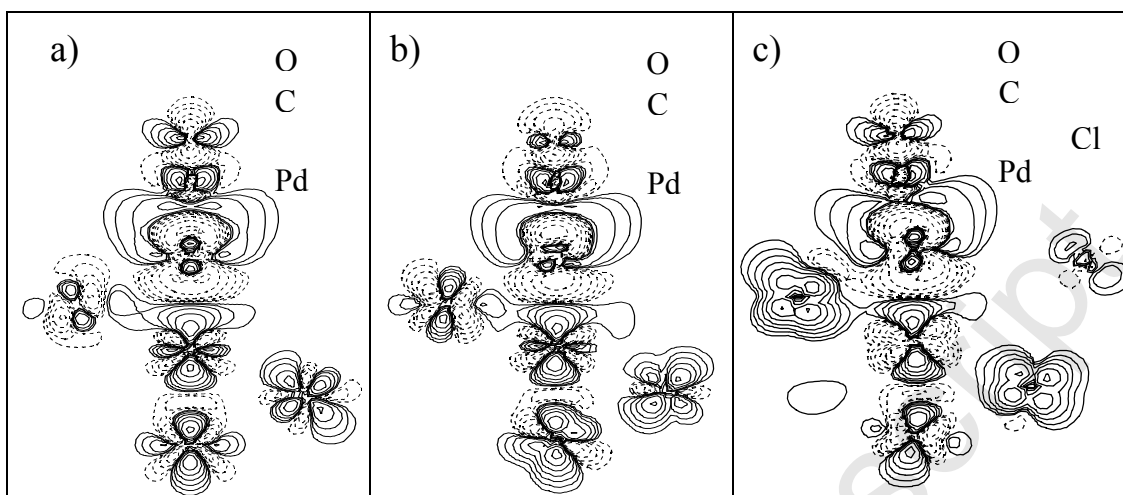
Figure 2.

Figure 3.

Figure 4.